Alternative Dewetting Pathways of Thin Liquid Films

Rachel Yerushalmi-Rozen,[1] Tobias Kerle,[2] Jacob Klein[2]

An alternative pathway for the initiation of dewetting in thin metastable films of partially miscible liquid mixtures is described. In this pathway, phase separation is followed by a dewetting process at the interface between the two phases. Dewetting proceeds (from the sample edges inward) as holes form. The initially smooth film breaks up into droplets at rates much faster than those allowed by classical rupture mechanisms. Marangoni flow appears to be responsible for the initiation of the flow of the dewetting front, and coupling between the flow in the two phases leads to accelerated hole formation.

The stability of thin liquid films on top of a solid surface is of importance for applications ranging from the lubrication of data storage devices to microlithographic resist films (*1*). Practical considerations frequently impose the choice of a liquid and a substrate that are not fully compatible, and the resulting film is unstable or metastable with a finite relaxation time. A relevant question is then, How long will the film retain its integrity before it ruptures and dewets? According to theories dealing with relaxation processes of the metastable state (*2*), the answer depends on the fastest available route for dewetting.

For single-component, nonvolatile thin films of nonpolar liquids, there are two classical dewetting routes: a process whereby van der Waals intermolecular forces amplify thermal fluctuations (often termed "spinodal dewetting") and a different pathway through which film rupture is induced by substrate contamination or imperfections that form nucleated holes (*3, 4*). In spinodal dewetting, the expectation time for holes to form, τ, is predicted to vary strongly with the film thickness h_0 as $\tau \sim h_0^5$. Heterogeneous nucleation is expected to be faster, especially in metastable films. Investigations (*5, 6*) reveal that dewetting of nonvolatile liquids on solid substrates exhibits the following common features, independent of the instability origin that initiates the rupture of holes: (i) Dewetting is initiated by the formation of round holes surrounded by a rim. (ii) The distribution of hole sizes over the entire sample at any given time is nearly monodisperse, which indicates that holes form within a very short time window. (iii) The areal density of holes is found to be constant over the entire sample (*5*). When the substrate is itself an (immiscible) liquid, viscous coupling at the liquid-liquid interface may modify the dewetting processes relative to the solid interface (*7*). Depending on the ratio of the viscosities of the two layers, the upper layer deforms the interface during the dewetting process. Partial miscibility of the two liquids is expected to result in a more complicated interplay between processes of phase separation and interfacial interactions.

We report experimental observations that suggest that thin films of binary mixtures of partially miscible liquids rupture and dewet by a very different pathway, associated with the growth of a directed dewetting front. Inside the miscibility gap, spontaneous phase separation into two coexisting liquid phases is followed by initiation of a dewetting front at the newly formed interface between them. The components of our liquid mixture are fully deuterated oligomeric styrene (dOS) and oligomeric ethylene-propylene (OEP) of molecular weights 580 and 2000, respectively (*8*). The viscosities of these Newtonian liquids at room temperature were determined as $\eta_{dOS} = 15$ poise (P) and $\eta_{OEP} = 50$ P, and the mixture has a (upper) critical temperature of $T = 368$ K, as estimated from cloud-point measurements. Apparent contact angles of 9° ± 0.5° and 8° ± 0.5° (of an OEP droplet on a liquid dOS substrate and a dOS droplet on a liquid OEP substrate, respectively) were measured by optical phase interference microscopy (*9*). Films of 80 to 800 nm in overall thickness were prepared by spin-casting from a mixture of the components at a concentration $\phi = 0.5$ on smooth gold-coated silicon wafers. Once cast on the wafers, the films were placed under an optical microscope and monitored under ambient conditions (23° ± 1°C). Composition-depth profiles of the thin films were measured with nuclear reaction analysis (NRA) (*10, 11*). This technique enables the direct measurement of the concentration-depth profile of a deuterated species within a nondeuterated environment. In our configuration, the technique yields resolutions of 10 and ~30 nm at the sample surface and at a depth of 400 nm, respectively.

Figure 1 shows the thin-film composition-depth profile (as recorded by NRA) of a symmetric mixture ($\phi = 0.5$) of OEP and dOS at 0.5 and 4 hours after preparation. The spectrum shows two layers with an interface aligned parallel to the substrate, as expected for demixed coexisting phases in this thickness range (*12, 13*). The steady state with respect to composition was reached in <30 min.

A typical example of the dewetting process of a thin film (400 nm), of the dOS/OEP mixture (Fig. 2) shows that dewetting proceeds through an inward advance of a dewetting front. This process is different to what is expected (and observed) in the dewetting of single-component films. In the system described here, as the dewetting front advances from the edges of the sample, hole formation occurs in a directed manner, proceeding from the edges toward the center, resulting in the collection of liquid and the formation of a rim. Ahead of this rim, new holes rupture. The area over which fresh holes rupture typically extends up to a few tenths of a millimeter ahead of the front. At a later time, depending on film thickness, the thin film is in a typical intermediate stage, with droplets forming at the outer regions of the films while the middle area of the sample remains

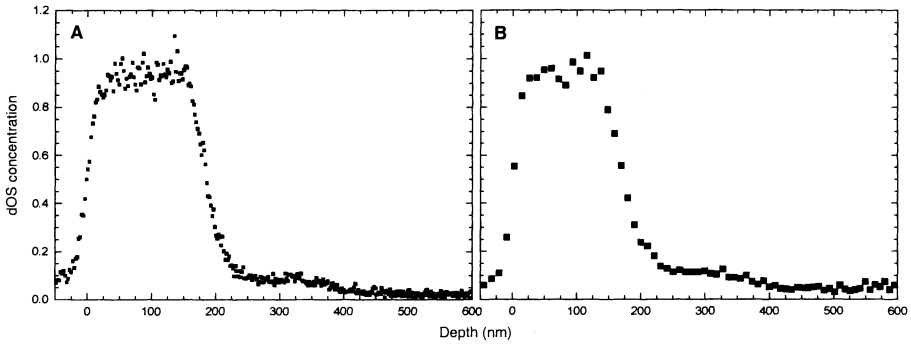

Fig. 1. Composition-depth profiles of dOS/OEP mixtures (**A**) 0.5 and (**B**) 4 hours after coating, as measured with NRA (*10, 11*). Although dewetting had already notably progressed in (B), the profile in the center area of the sample that was not yet dewetted could be measured by focusing the profiling ion beam into that area. Both profiles show a dOS-rich ($\phi = 0.9$) layer close to the air surface and a dOS-poor ($\phi = 0.1$) layer below.

[1]Department of Chemical Engineering, Ben-Gurion University of the Negev, 84105 Beer-Sheva, Israel. [2]Department of Materials and Interfaces, Weizmann Institute of Science, 76100 Rehovot, Israel.

visually smooth and unperturbed. After ~12 hours, the entire surface is covered with droplets (Fig. 2F), with an average diameter that decays toward the center of the sample. The areal density of holes increases toward the center of the sample, and the rate of hole formation is much faster than that in single-component films of a similar thickness.

An intermediate stage of the dewetting process in a thicker film (800 nm) of the same initial composition (Fig. 3A) shows that the retracting top layer exposes a lower thin liquid layer rather than the gold substrate. The shape of the propagating front preserves the geometry of the sample, and the mean velocity of the rim is comparable to the growth velocity of the holes themselves (1 μm/min).

Special attention should be given to the rupture of holes ahead of the front (Fig. 3B). In Fig. 4, we present the distribution of hole diameters as a function of the distance from the dewetting front in a sample such as that shown in Fig. 3B. In contrast to classical schemes of dewetting, where holes of nearly equal diameter are spread over the entire sample, the mechanism described here exhibits holes of similar diameter only in a narrow region of the film. With increasing distance from the dewetting front, the average hole diameter decreases roughly exponentially. The sharp distribution of hole diameters within a given region indicates that hole rupture occurred only during a narrow time window, because of the propagation of the front; the locus of newly ruptured holes precedes the dewetting rim.

A detailed analysis of dewetting and spreading at a liquid-liquid interface was presented by Brochard-Wyart and co-workers (*7, 14*) and by Joanny (*15*). At the limit of a high-viscosity subphase, the expected characteristic rupture time is similar to that of the solid-liquid case. At the limit of low viscosity, dewetting is accelerated by the fluidity of the substrate, which allows flow (and thus viscous dissipation) in the lower film (*7*). Although the rupture time is predicted to be somewhat shorter than that in the case of a solid-fluid interface, dewetting is essentially still expected to proceed through one of the two classical routes.

The dewetting process described here, however, is distinguished by the following features: the initiation of the growing dewetting front at the sample edges, the subsequent accelerated rupture of holes ahead of this front, and the associated hole growth and dewetting. The spin-coating process causes the sample edges to differ from the bulk in two aspects: (i) The edge acts as a sharp discontinuity in the otherwise continuous film; a rim of the liquid accumulates at the sample edges and forms a region of thicker film. (ii) The differences in viscosity and solubility of the two fluids in the casting solvent lead to enrichment of the rim by the lower viscosity component (dOS in this case). To decouple the influence of these effects, we performed two sets of experiments. In the first set, we simulated the edge effect by creating an elongated rimmed depression at the center of the smooth film of the as-cast mixture to form an artificial thickness gradient. No new dewetting front was initiated at this line. In the second set, a macroscopic droplet of dOS was placed at the center of a precast film of the symmetric dOS/OEP mixture to create a local concentration gradient. A second dewetting front starting from the dOS droplet developed and propagated outward with time. It is well known (*16, 17*) that gradients ($d\gamma/dx$) in interfacial tension γ (with distance x), generated by composition gradients, can lead to the evolution of a Marangoni flow that induces a net mass transport in the interfacial plane (as illustrated in Fig. 5A). For a weakly curved surface, the shear velocity v_x of the liquid (viscosity η) from the sample edge inward may be described by the relation $v_x = (h/2\eta)(d\gamma/dx)$, which gives an upper limit value of 6 μm/min (*18*), comparable to the

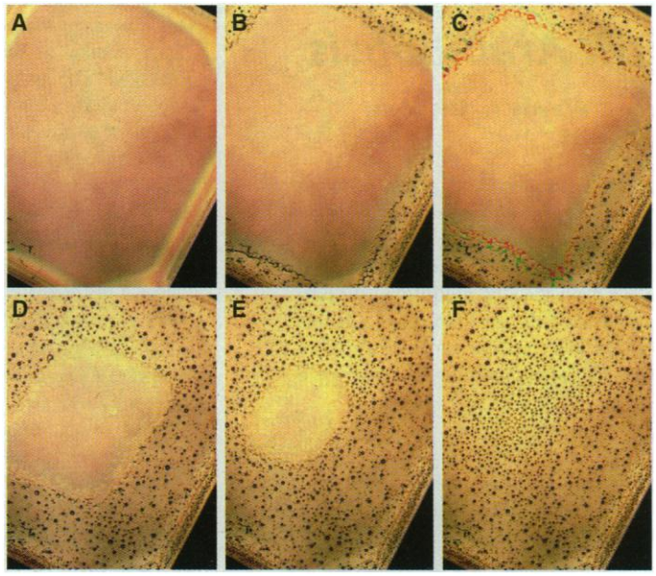

Fig. 2. Time evolution of the dewetting process of (**A**) a 400-nm-thick dOS/OEP film cast from a 50% solution. A dewetting front starting at the sample edges propagates inward, leaving droplets on the dewetted area. Propagation after (**B**) 1.5, (**C**) 3.0, (**D**) 6.0, (**E**) 9.0, and (**F**) 12 hours. The scale of each image panel is 1 cm by 1.5 cm.

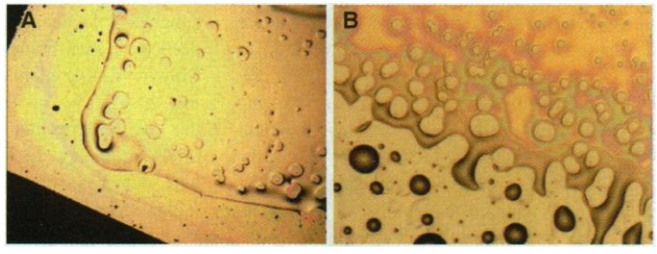

Fig. 3. (**A**) Intermediate stage of the same process shown in Fig. 2 in a sample with twice the thickness of the original sample. A rim forms at the edges of the retracting dOS film. The scale of the image is 1.5 cm by 1 cm. (**B**) A sample prepared in an analogous way to the one presented in Fig. 2. The magnification is 10 times greater than that in (A).

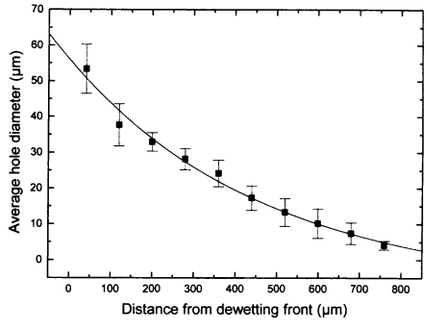

Fig. 4. Average hole diameter as a function of the distance from the dewetting front. To calculate the average hole diameter, we measured all holes within 90-μm strips. Error bars represent the statistical deviation of the hole diameters.

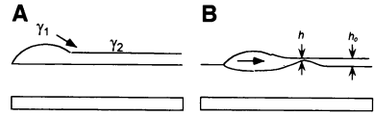

Fig. 5. Schematic model of a possible mechanism connecting the motion of the liquid rim with the accelerated hole rupture ahead of it. As the rim begins to move (**A**), its flow distorts the lower film, leading to a wave of the substrate liquid forming ahead of the moving droplet. This front thins the upper layer [as in (**B**)], creating a line of "preferred breakup points" ahead of the dewetting front.

observed initial velocity (~3 μm/min) of the front. Thus, the gradient of chemical potential rather than the thickness gradient is responsible for initiating the growing dewetting front. Once the dewetting front advances, one would expect the driving force exerted by the Marangoni flow to decay. The front, however, continues to move, driven by the reduction in free energy associated with progressive exposure of the lower layer.

In Fig. 5B, we schematically show a possible mechanism, suggested by the above results, connecting the motion of the liquid rim with the accelerated hole rupture ahead of it. A liquid drop or a rim resting on a liquid substrate will deform the contact area between the two fluids. As the rim begins to move, its flow distorts the lower film and leads to a wave of the substrate liquid forming ahead of the moving droplet. Similarly, a droplet spreading on top of another liquid leads to the formation of a wave ahead of the spreading precursor film. The wave locally thins the upper layer to a thickness $h < h_0$, the unperturbed thickness, to form a zone of higher rupture probability (recalling that, for a spinodal dewetting process, $\tau \sim h^5$). This mechanism results in a line of "preferred breakup points" ahead of the dewetting front and qualitatively explains both the directed growth and the variation of hole diameters shown in Fig. 3. For the case of liquid mixtures, this process represents an alternative and more rapid pathway to the classical processes associated with spinodal dewetting or with heterogeneous nucleation mechanisms.

References and Notes

1. P. Weiss, *Sci. News* **155**, 28 (1999).
2. K. Binder, *Rep. Prog. Phys.* **50**, 783 (1987).
3. L. Leger and J. F. Joanny, *ibid.* **55**, 431 (1992).
4. F. Brochard-Wyart, J. M. diMeglio, D. Quéré, P. G. deGennes, *Langmuir* **7**, 335 (1991); F. Brochard-Wyart and J. Daillant, *Can. J. Phys.* **68**, 1084 (1990).
5. See, for example, S. Herminghaus *et al.*, *Science* **282**, 916 (1998); G. Reiter, *Langmuir* **9**, 1344 (1993); T. G. Stange, D. F. Evans, W. A. Hendrickson, *ibid.* **13**, 4459 (1997); J. Bischof, D. Scherer, S. Herminghaus, P. Leiderer, *Phys. Rev. Lett.* **77**, 1536 (1996); K. Jacobs, S. Herminghaus, K. Mecke, *Langmuir* **14**, 965 (1998).
6. R. Xie, A. Karim, J. F. Douglas, C. C. Han, R. A. Weiss, *Phys. Rev. Lett.* **81**, 1251 (1998).
7. F. Brochard-Wyart, P. Martin, C. Redon, *Langmuir* **9**, 3682 (1993).
8. We observed a qualitatively similar phenomenon with the nondeuterated oligomers OS-OEP. In that system, the OEP-rich phase aligns at the air interface, and the OS-rich phase aligns at the gold surface.
9. White-light interference microscopy (NewView 200, Zygo, Middlefield, CT) was used for profiling the detailed shape of a liquid droplet on top of the liquid film. In this three-dimensional technique, an image of the surface is obtained by analyzing the interference pattern formed by a reference and a sample beam. The technique provides a detailed profile of the contact line with subnanometric resolution in the vertical direction and micrometer resolution in the lateral direction.
10. T. Kerle *et al.*, *Acta Polym.* **48**, 548 (1997).
11. U. K. Chaturvedi *et al.*, *Appl. Phys. Lett.* **56**, 1228 (1990).
12. F. Scheffold *et al.*, *J. Chem. Phys.* **104**, 8786 (1996).
13. K. Binder, *ibid.* **79**, 6387 (1983).
14. F. Brochard-Wyart, G. Debregeas, P. G. deGennes, *Colloid Polym. Sci.* **274**, 70 (1996).
15. J. F. Joanny, *Physicochem. Hydrodyn.* **9**, 183 (1987).
16. H. Linde *et al.*, *J. Colloid Interface Sci.* **188**, 16 (1997).
17. X. Fanton and A. M. Cazabat, *Langmuir* **14**, 2554 (1998).
18. With $h = 200 \times 10^{-9}$ m, $\eta = 50$ P, $\delta\gamma = 2 \times 10^{-3}$ N/m, and $\delta x = 1$ mm, shear velocity $v_x = 6$ μm/min.

19. We are grateful to L. J. Fetters and M. Wilhelm for kindly donating the OEP and dOS oligomers. We thank J. F. Joanny, S. Safran, and H. Grüll for enlightening discussions and the U.S.–Israel Binational Science Foundation (grant 95-147), the Wolfson Family Charitable Trust (to R.Y.-R.), the German-Israel Foundation (grant I-568-275.0597), and the Israel Ministry of Science (Tashtiot Program) for support.

12 April 1999; accepted 9 July 1999

Salt Tolerance Conferred by Overexpression of a Vacuolar Na^+/H^+ Antiport in *Arabidopsis*

Maris P. Apse,* Gilad S. Aharon,* Wayne A. Snedden, Eduardo Blumwald†

Agricultural productivity is severely affected by soil salinity. One possible mechanism by which plants could survive salt stress is to compartmentalize sodium ions away from the cytosol. Overexpression of a vacuolar Na^+/H^+ antiport from *Arabidopsis thaliana* in *Arabidopsis* plants promotes sustained growth and development in soil watered with up to 200 millimolar sodium chloride. This salinity tolerance was correlated with higher-than-normal levels of *AtNHX1* transcripts, protein, and vacuolar Na^+/H^+ (sodium/proton) antiport activity. These results demonstrate the feasibility of engineering salt tolerance in plants.

Salinity stress is one of the most serious factors limiting the productivity of agricultural crops. The detrimental effects of salt on plants are a consequence of both a water deficit resulting in osmotic stress and the effects of excess sodium ions on critical biochemical processes (*1*). In order to tolerate high levels of salt, plants should be able to utilize ions for osmotic adjustment and internally distribute these ions to keep sodium away from the sites of metabolism (*1*). Plant cells are structurally well suited for the sequestration of ions because of the presence of large, membrane-bound vacuoles. It has been proposed that in salt-tolerant plants, the compartmentation of Na^+ into vacuoles, through the operation of a vacuolar Na^+/H^+ antiport, provides an efficient mechanism to avert the deleterious effects of Na^+ in the cytosol and maintains osmotic balance by using Na^+ (and chloride) accumulated in the vacuole to drive water into the cells (*2*). This Na^+/H^+ antiport transports Na^+ into the vacuole by using the electrochemical gradient of protons generated by the vacuolar H^+-translocating enzymes, H^+–adenosine triphosphatase (ATPase) and H^+–inorganic pyrophosphatase (PP_iase) (*3, 4*). Vacuolar Na^+/H^+ antiport activity was shown first in tonoplast vesicles from red beet storage tissue (*5*) and later in various halophytic and salt-tolerant glycophytic species (*6, 7*). Chloride transport into the vacuole is mediated by anion channels (*8*). In *Arabidopsis*, a vacuolar chloride channel, AtCLCd, similar to the yeast Gef1, has been cloned (*9*). The analysis of genes involved in cation detoxification in yeast led to the identification of a novel Na^+/H^+ antiport (Nhx1). Nhx1 was localized to a prevacuolar compartment and showed a high degree of amino acid sequence similarity to Na^+/H^+ antiports from *Caenorhabditis elegans* and humans (NHE6, mitochondrial) (*10*). Recently, the *Arabidopsis thaliana* genome-sequencing project has allowed for the identification of a plant gene (*AtNHX1*) homologous to the *Saccharomyces cerevisiae Nhx1* gene product (*11–13*). Both Nhx1 and Gef1 are localized to the yeast prevacuolar compartment, suggesting a role for this compartment in salt tolerance. Overexpression of *AtNHX1* suppresses some of the salt-sensitive phenotypes of the Δ*nhx1* yeast strain (*13*), suggesting that the plant and the yeast gene products might be functionally similar.

AtNHX1 transcripts are found in root, shoot, leaf, and flower tissues (*11*). To determine the subcellular localization of AtNHX1, we immunoblotted membrane fractions (*14*) isolated from wild-type plants and plants overexpressing AtNHX1 (*15*) with antibodies raised against the COOH-terminus of AtNHX1 (Fig. 1). A protein of an apparent molecular mass of 47 kD was detected mainly in the tonoplast- and Golgi/endoplasmic reticulum (ER)–enriched fractions, and was more abundant in the transgenic plants. No noticeable cross-reactivity

Department of Botany, University of Toronto, 25 Willcocks Street, Toronto, Ontario M5S 3B2, Canada.

*These authors contributed equally to this work.
†To whom correspondence should be addressed. E-mail: blumwald@botany.utoronto.ca